Reversible Bond Formation and Cleavage of the Oxo Bridge of $[Ru_2(\mu\text{-}O)(dioxolene)_2(btpyxa)]^{3+}$ [btpyxa = 2,7-Di-*tert*-butyl-9,9-dimethyl-4,5-bis(2,2′:6′,2′′-terpyrid-4′-yl)xanthene] Driven by a Three-Electron Redox Reaction

Tohru Wada[a] and Koji Tanaka*[a]

Keywords: Electronic structure / O ligands / Oxidation / Reduction / Ruthenium

The bis(chlororuthenium) complex $[Ru_2Cl_2(3,6\text{-}tBu_2sq)_2(btpyxa)](PF_6)_2$ [**1**]$(PF_6)_2$ [3,6-tBu_2sq = 3,6-di-*tert*-butyl-1,2-benzosemiquinone; btpyxa = 2,7-di-*tert*-butyl-9,9-dimethyl-4,5-bis(2,2′:6′,2′′-terpyrid-4′-yl)xanthene] and the oxo-bridged diruthenium complex $[Ru_2(\mu\text{-}O)(3,6\text{-}tBu_2sq)_2(btpyxa)](PF_6)_3$ [**2**]$(PF_6)_3$ were synthesized, and the redox behavior of these complexes, which contain a non-innocent dioxolene ligand, was investigated by electrochemical and electrospectrochemical methods. Dicationic $[\mathbf{1}]^{2+}$ undergoes two successive metal-centered one-electron and a simultaneous two-electron ligand-based redox reaction at $E_{1/2}$ = +0.13 and +0.09 and $E_{1/2}$ = –0.75 V (vs. SCE), respectively, in CH_2Cl_2. The UV/Vis/NIR spectrum of tricationic $[\mathbf{2}]^{3+}$ shows an intervalence-transition (IT) band at 1333 nm (ε = 1.52×10^4 M^{-1} cm^{-1}) in a near-IR region together with two CT bands at 766 (ε = 2.21×10^4 M^{-1} cm^{-1}) and 586 nm (ε = 1.13×10^4 M^{-1} cm^{-1}) in CH_2Cl_2. The mixed-valence complex of $[\mathbf{2}]^{3+}$ with an Ru^{IV}–O–Ru^{III} core is reversibly oxidized and reduced to the Ru^{IV}–Ru^{IV} and Ru^{III}–Ru^{III} oxidation states at $E_{1/2}$ = +0.63 and –0.01 V, respectively, in CH_2Cl_2. On the other hand, three-electron reduction of [**2**]$(PF_6)_3$ is accompanied by the cleavage of the Ru–O–Ru bond at E_p = +0.02 V to give $[\{Ru(OMe)(3,5\text{-}tBu_2sq)\}\{Ru(OH_2)(3,5\text{-}tBu_2sq)\}(btpyxa)]^+$ in MeOH.

Introduction

Much attention has been paid to transition-metal complexes with non-innocent ligands such as dioxolenes, dithiolenes, and benzoquinonediimines due to their unique electronic,[1] magnetic,[2] and structural[3] properties that derive from pπ–dπ interactions between the metals and such ligands. Ruthenium–dioxolene complexes, in particular, have strong pπ–dπ interactions because of the close orbital energies between the central metal and the dioxolene ligand. Indeed, the electronic structures of ruthenium–dioxolene complexes are characterized in terms of charge distribution due to delocalization of π-electrons over the central metal and the ligand.[4,5] We have demonstrated that the dioxolene ligand in $[Ru(L)(3,5\text{-}tBu_2sq)(trpy)]^{2+}$ [L = OH_2,[6] CO,[7] 3,5-tBu_2sq (3,5-di-*tert*-butyl-1,2-benzosemiquinone), trpy (2,2′:6′,2′′-terpyridine)] exerts an unusually strong influence on the electronic states of the ligand L. For example, an aqua ligand of $[Ru^{III}(OH_2)(3,5\text{-}tBu_2sq)(trpy)]^{2+}$ dissociates two protons under strongly basic conditions to give the corresponding terminal ruthenium oxo complex $[Ru^{II}(O^{\cdot-})(3,5\text{-}tBu_2sq)(trpy)]^0$ without forming a μ-oxo diruthenium complex (Scheme 1).[6] EPR measurements revealed the radical character of the oxo ligand of the resultant oxo complex. Unusual oxyl radical formation results from intramolecular one-electron transfer from the doubly deprotonated aqua ligand of $[Ru^{III}(OH_2)(3,5\text{-}tBu_2sq)(trpy)]^{2+}$ to the Ru^{III}-semiquinone framework. A similar conversion of two hydroxyl ligands into two oxyl radicals in the bis(ruthenium–dioxolene) complex $[Ru_2(OH)_2(3,6\text{-}tBu_2q)_2(btpyan)]^{2+}$ [3,6-tBu_2q = 3,6-di-*tert*-butyl-1,2-benzoquinone, btpyan = 1,8-bis(2,2′:6′,2′′-terpyrid-4′-yl)anthracene], in which two ruthenium-dioxolene frameworks are fixed in a face-to-face conformation by the rigid btpyan ligand, enabled the catalytic four-electron oxidation of water through O–O bond formation by the radical coupling of the two oxyl radical ligands.[8]

We synthesized two new complexes, a bis(chlororuthenium–dioxolene) complex $[\mathbf{1}]^{2+}$ and a μ-oxo-bis(ruthenium–dioxolene) complex $[\mathbf{2}]^{3+}$ bridged by 2,7-di-*tert*-butyl-9,9-dimethyl-4,5-bis(2,2′:6′,2′′-terpyrid-4′-yl)xanthene (btpyxa) in which two terpyridines are linked by a xanthene skeleton (Scheme 2). The two terpyridine units bridged by a xanthene and an anthracene moiety in btpyxa and btpyan, respectively, are not able to rotate freely because of their steric repulsions.[8,9] The distinct difference between btpyxa and btpyan is that the sp^3 carbon and oxygen atoms at the 9- and 10-position of xanthene, respectively, in the former

[a] Institute for Molecular Science and CREST, Japan Science and Technology Agency (JST),
Higashiyama 5-1, Myodaiji, Okazaki, Aichi 444-8787, Japan
E-mail: ktanaka@ims.ac.jp

  DOI: 10.1002/ejic.200500141

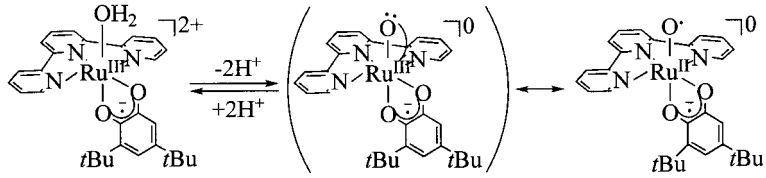

Scheme 1. Acid-base equilibrium of the aqua complex $[Ru(OH_2)(3,5\text{-}tBu_2sq)(trpy)]^{2+}$ and the oxyl radical complex $[Ru(O)(3,5\text{-}tBu_2sq)(trpy)]^{0}$.

give flexibility of the unit, whereas the anthracene in the latter has a rigid planar structure. Complexes $[\mathbf{1}]^{2+}$ and $[\mathbf{2}]^{3+}$ have the same skeleton fixed by btpyxa, but their electronic states and redox behavior are quite different from each other. We will report here the electronic structures of the diruthenium complexes and redox reactions accompanied with the Ru–O–Ru bond cleavage.

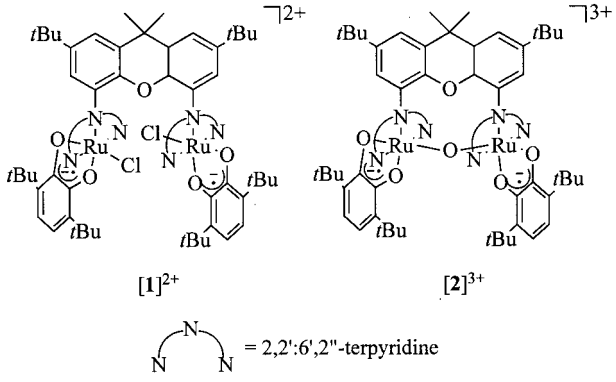

Scheme 2. Schematic structures of $[\mathbf{1}]^{2+}$ and $[\mathbf{2}]^{3+}$.

Results and Discussion

Syntheses and Electronic Structures

The reaction of $[Ru_2Cl_6(btpyxa)]$ with two equivalents of 3,6-di-*tert*-butylcatechol in the presence of *t*BuOK in MeOH gave a purple solution, presumably due to the formation of a bis[ruthenium(II) semiquinone] complex under N_2. The purple solution gradually turned blue upon exposure to air. The crude product was purified by column chromatography on alumina and subsequent treatment with aqueous NH_4PF_6. The product is a dicationic diruthenium complex containing two chloride ligands $\{[\mathbf{1}](PF_6)_2\}$. The UV/Vis/NIR spectrum of $[\mathbf{1}](PF_6)_2$ in CH_2Cl_2 [Figure 1(a)] shows a strong band at 598 nm ($\varepsilon = 1.93 \times 10^4\ M^{-1}cm^{-1}$) assignable to a charge-transfer (CT) band resulting from the $Ru^{III}(sq)$ (sq = semiquinone) framework by analogy with the electronic spectra of the analogous $[Ru^{III}(OH_2)(3,5\text{-}tBu_2sq)(trpy)]$.[6b] The resonance Raman spectrum of $[\mathbf{1}](PF_6)_2$ exhibits two strongly enhanced bands at 1357 and 1158 cm^{-1} upon excitation at 632.8 nm, whereas the intensities of these bands decrease upon excitation at 514.5 nm. In addition, the stretching modes of the semiquinone of $[Ru^{III}(OH_2)(3,5\text{-}tBu_2sq)(trpy)]^{2+}$ are found at 1353 and 1167 cm^{-1}.[6b] The strong absorption band of $[\mathbf{1}]^{2+}$ at 598 nm, therefore, is reasonably assigned to the CT band of the $Ru^{III}(sq)$ core. Thus, two ruthenium-dioxolene frameworks of $[\mathbf{1}]^{2+}$ have the $Ru^{III}(sq)$ oxidation state, although the contribution of an $Ru^{II}(q)$ (q = quinone) framework cannot be ignored in the electronic structure of $[\mathbf{1}]^{2+}$.

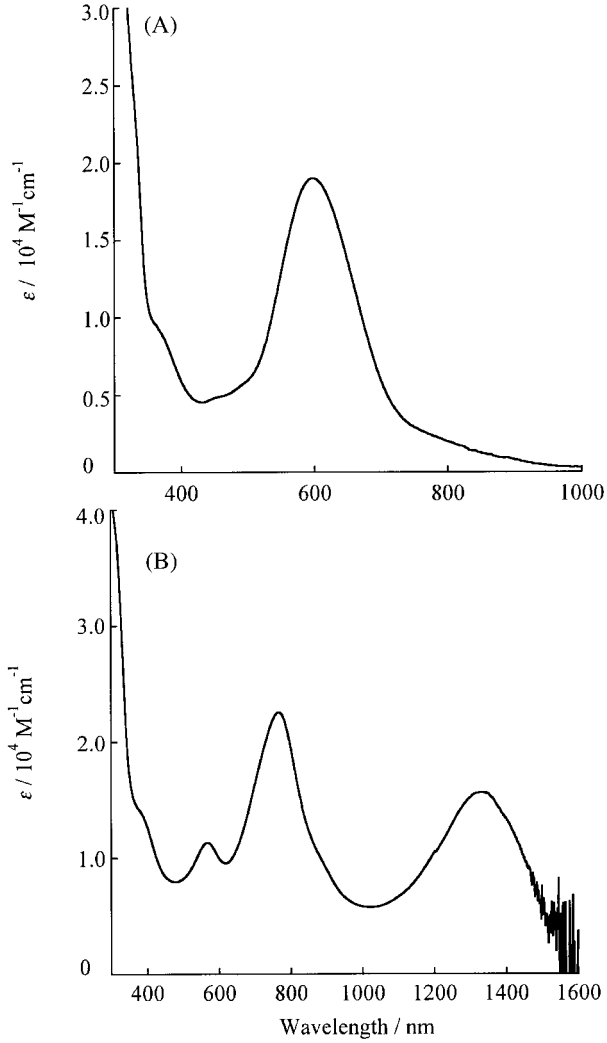

Figure 1. UV/Vis/NIR spectra of (A) $[\mathbf{1}](PF_6)_2$ and (B) $[\mathbf{2}](PF_6)_3$ in CH_2Cl_2.

We noticed the formation of a small amount of an oxo-bridged diruthenium complex $[\mathbf{2}]^{3+}$ as a minor product in the reaction of $[Ru_2Cl_6(btpyxa)]$ with 3,6-di-*tert*-butylcatechol in MeOH. The yield of $[\mathbf{2}](PF_6)_3$ was dependent on

contamination of water in MeOH, suggesting that the bridging oxygen of $[\mathbf{2}]^{3+}$ comes from H_2O. The reaction of $[Ru_2(\mu\text{-}O)Cl_2(btpyxa)]$ with 3,6-di-*tert*-butylcatechol in the presence of a large excess of KOAc, followed by treatment with $NaPF_6$ in MeOH, gave $[\mathbf{2}](PF_6)_3$ in a low yield of 11%. The fact that no oxo-bridged species (Ru–O–Ru) were detected in the synthesis of the 1,8-bis(terpyridyl)anthracene-bridged complex $[Ru_2(OH)_2(3,6\text{-}t\text{Bu}_2\text{sq})_2(btpyan)]^{2+}$[8] is explained by the greater flexibility of the xanthene skeleton of btpyxa compared with the anthracene in btpyan. The UV/Vis/NIR spectrum of $[\mathbf{2}](PF_6)_3$ [Figure 1(b)] in CH_2Cl_2 shows a strong band at 1333 nm ($\varepsilon = 1.52\times10^4$ M^{-1}cm^{-1}) assigned to the intervalence-transition (IT) band (vide infra) in the near-IR region, with two CT bands at 766 ($\varepsilon = 2.21\times10^4$ M^{-1}cm^{-1}) and 586 nm ($\varepsilon = 1.13\times10^4$ M^{-1}cm^{-1}) in the visible region. The appearance of the IT band at 1333 nm indicates that $[\mathbf{2}]^{3+}$ is a mixed-valence complex. The contribution of $[(sq)Ru^{III}\text{–}O\text{–}Ru^{IV}(sq)]^{3+}$, therefore, is much higher than other resonance forms such as $[(q)Ru^{II}\text{–}O\text{–}Ru^{III}(q)]^{3+}$, $[(cat)Ru^{IV}\text{–}O\text{–}Ru^{IV}(sq)]^{3+}$ (cat = catecholato), etc. in the electronic structure of $[\mathbf{2}]^{3+}$.

Redox Behavior of $[\mathbf{1}]^{2+}$ and $[\mathbf{2}]^{3+}$ in CH_2Cl_2

The cyclic voltammogram (CV) of $[\mathbf{1}](PF_6)_2$ in CH_2Cl_2 shows three pairs of anodic and cathodic waves in a potential range from +0.8 to –1.3 V (vs. SCE; Figure 2).

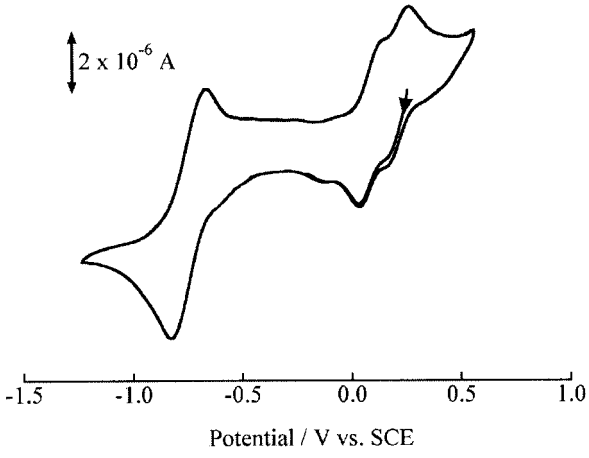

Figure 2. CV of $[\mathbf{1}](PF_6)_2$ in CH_2Cl_2 containing $n\text{Bu}_4NClO_4$ (0.1 M) as an electrolyte under N_2. The arrows indicate the rest potential of the solution and the direction of scan.

Based on the rest potential (+0.26 V) of $[\mathbf{1}]^{2+}$ in CH_2Cl_2, the two quasi-reversible redox couples at $E_{1/2}(1) = +0.13$ and $E_{1/2}(2) = +0.09$ V are associated with the metal-centered redox reactions. The redox couple at $E_{1/2}(3) = -0.75$ V with large peak currents is consistent with a dioxolene-based redox reaction due to its similarity to the redox potential of the analogous monomer [RuCl(3,5-$t\text{Bu}_2$sq)(trpy)].[5] The bulk electrolysis of $[\mathbf{1}]^{2+}$ in CH_2Cl_2 at +0.00 V consumes 2.03 F mol^{-1} of electricity. In addition, 2.01 F mol^{-1} of electricity also passes in the subsequent electrolysis of the resultant solution at –0.75 V.[10] The two redox reactions at $E_{1/2} = +0.13$ and +0.09 V apparently result from a one-electron transfer process because of the similarity of the peak currents of both redox waves (Figure 2). On the other hand, the redox couple at –0.75 V is a simultaneous two-electron transfer. The redox reactions at $E_{1/2}(1) = +0.13$, $E_{1/2}(2) = +0.09$, and $E_{1/2}(3) = -0.75$ V are summarized in Scheme 3.

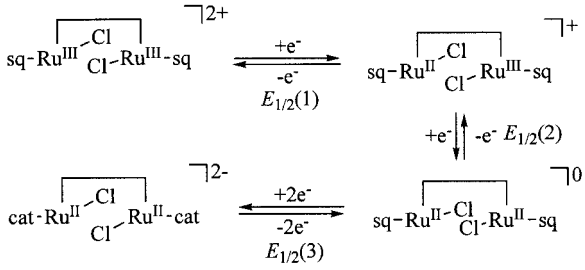

Scheme 3. Redox reactions of $[\mathbf{1}]^{2+}$ in CH_2Cl_2.

The equilibrium constant (K_d) for the disproportionation reaction of $[\mathbf{1}]^+$ is defined by Equations (1) and (2).[11] The K_d calculated from $\Delta E_{1/2} = E_{1/2}(2) - E_{1/2}(1) = -0.04$ V is 0.21, which proves that the mixed-valence complex $[\mathbf{1}]^+$ ($Ru^{II}\text{–}Ru^{III}$) exists as an equilibrium mixture of $[\mathbf{1}]^{2+}$ and $[\mathbf{1}]^0$ in solution.

$$2[\mathbf{1}]^+ \overset{K_d}{\rightleftarrows} [\mathbf{1}]^0 + [\mathbf{1}]^{2+} \quad (1)$$

$$E_{1/2}(2) - E_{1/2}(1) = \frac{RT}{F}\ln K_d \quad (2)$$

Electrospectroscopy of $[\mathbf{1}]^{2+}$ in CH_2Cl_2 (Figure 3) also provides valid information about the $[\mathbf{1}]^{2+}/[\mathbf{1}]^+$ and $[\mathbf{1}]^+/[\mathbf{1}]^0$ redox reactions.

The CT band at 598 nm of $[\mathbf{1}]^{2+}$ decreases by half in the electrochemical reduction at +0.10 V and a new band appears at 882 nm, which is assigned to a CT band resulting from the $Ru^{II}(sq)$ moiety. The 598-nm band disappears completely in the electrolysis at –0.10 V and the 882-nm band is shifted to 866 nm with an increase in its absorbance. The shift of the CT band from 598 nm to 882 nm and then to 866 nm upon the reduction of $[\mathbf{1}]^{2+}$ at +0.10 V and –0.10 V is ascribed to the changes of the electronic structures from $[(sq)ClRu^{III}\text{–}Ru^{III}Cl(sq)]^{2+}$ to $[(sq)ClRu^{III}\text{–}Ru^{II}Cl(sq)]^0$ through $[(sq)ClRu^{II}\text{–}Ru^{III}Cl(sq)]^+$. Further reduction of $[\mathbf{1}]^0$ at –1.0 V completely extinguished the 866-nm band of $[(sq)ClRu^{II}\text{–}Ru^{II}Cl(sq)]^0$. Taking into account that the $Ru^{II}(cat)$ framework, with a fully occupied Ru t_{2g} and π orbital (π* orbital of quinone), has no CT band between Ru and the dioxolene ligand, the $[\mathbf{1}]^0/[\mathbf{1}]^{2-}$ couple at –0.75 V is assigned to the simultaneous two-electron reduction of $[(sq)ClRu^{II}\text{–}Ru^{II}Cl(sq)]^0$ to $[(cat)ClRu^{II}\text{–}Ru^{II}Cl(cat)]^{2+}$. The spectral changes in the redox cycle between $[\mathbf{1}]^{2+}$, $[\mathbf{1}]^+$, $[\mathbf{1}]^0$, and $[\mathbf{1}]^{2-}$ take place reversibly, since re-oxidation of a CH_2Cl_2 solution of $[\mathbf{1}]^{2-}$ at +0.4 V fully restored the spectrum of $[\mathbf{1}]^{2+}$. It is worthy of note that $[\mathbf{1}]^{2+}$ displays two Ru^{II}/Ru^{III} redox couples at $E_{1/2}(1) = +0.13$ and $E_{1/2}(2) = +0.09$ V, while the two semiquinone ligands of $[\mathbf{1}]^0$ are reduced to catecholato ones at the same potential. However,

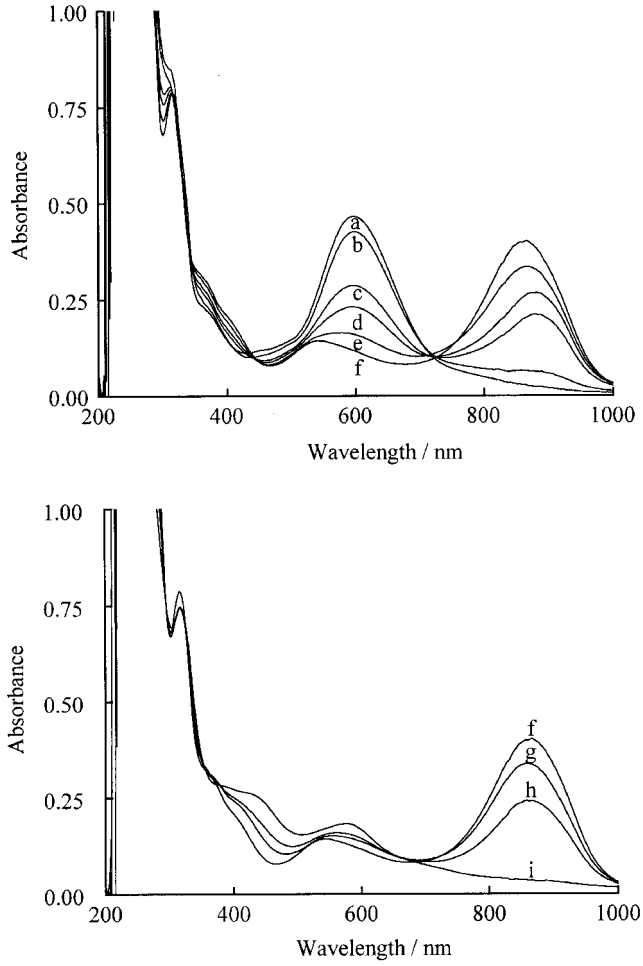

Figure 3. UV/Vis/NIR spectra of $[\mathbf{1}](PF_6)_2$: a) before electrolysis and after electrolysis at b) +0.20 V, c) +0.15 V, d) +0.10 V, e) +0.05 V, f) 0.00 V, g) –0.70 V, h) –0.80 V, and i) –0.90 V in CH_2Cl_2 containing nBu$_4$NClO$_4$ (0.1 M) as an electrolyte.

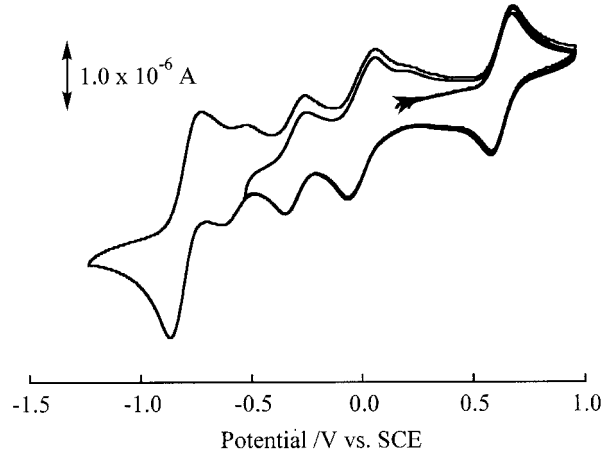

Figure 4. CV of $[\mathbf{2}](PF_6)_3$ in CH_2Cl_2 containing nBu$_4$NClO$_4$ (0.1 M) as an electrolyte under N_2. The arrows indicate the rest potential of the solution and the direction of scan.

the IT band associated with $[\mathbf{1}]^+$, which was generated by the bulk electrolysis of $[\mathbf{1}]^{2+}$ at +0.10 V in CH_2Cl_2, was not detected at all in the region from 500 to 2200 nm. Meyer at al. have demonstrated that electrostatic effects caused by charge differences of dinuclear complexes result in a discrepancy of the redox potentials of two redox sites by about 20–60 mV.[12] The absence of the IT band of $[\mathbf{1}]^{2+}$ and a small potential difference between the two Ru^{II}/Ru^{III} redox couples (ΔE = 40 mV), therefore, may be ascribed to electrostatic effects, although an electronic interaction between the two Ru atoms of the $[(sq)Ru^{II}Cl\ ClRu^{III}(sq)]^+$ framework cannot be ruled out completely.

The oxo-bridged diruthenium complex $[\mathbf{2}]^{3+}$ exhibits a strong IT band at 1333 nm and two strong CT bands at 766 and 578 nm, as described above. The actual electronic structure of $[\mathbf{2}]^{3+}$ is approximated by $[(sq)Ru^{III}–O–Ru^{IV}(sq)]^{3+}$, since the strong electron-donating ability of the μ-oxo group in $[\mathbf{2}]^{3+}$ would stabilize higher oxidation states of Ru. Indeed, the redox behavior of $[\mathbf{2}]^{3+}$ is very different from that of $[\mathbf{1}]^{2+}$ (compare Figures 2 and 4).

The CV of $[\mathbf{2}]^{3+}$ (Figure 4) shows four quasi-reversible redox couples at $E_{1/2}(1)$ = +0.63, $E_{1/2}(2)$ = –0.01, $E_{1/2}(3)$ = –0.30, and $E_{1/2}(4)$ = –0.80 V. The redox reactions at $E_{1/2}(1)$ = +0.63 and $E_{1/2}(2)$ = –0.01 V were assigned to the $[(sq)Ru^{III}–O–Ru^{IV}(sq)]^{3+}/[(sq)Ru^{IV}–O–Ru^{IV}(sq)]^{4+}$ and the $[(sq)Ru^{III}–O–Ru^{IV}(sq)]^{3+}/[(sq)Ru^{III}–O–Ru^{III}(sq)]^{2+}$ couples, respectively, on the basis of the rest potential of the solution (E_{rest} = +0.21 V). The pattern and the potential of the redox couple at $E_{1/2}(1)$ = –0.80 V of $[\mathbf{2}]^{3+}$ are close to those of the simultaneous two-electron reduction of the two semiquinone ligands of $[\mathbf{1}]^{2+}$. Therefore, the redox reaction at $E_{1/2}(3)$ = –0.30 V is correlated with the $[(sq)Ru^{III}–O–Ru^{III}(sq)]^{2+}/[(sq)Ru^{III}–O–Ru^{II}(sq)]^+$ couple. The redox reactions of $[\mathbf{2}]^{3+}$ in CH_2Cl_2 are summarized in Scheme 4.

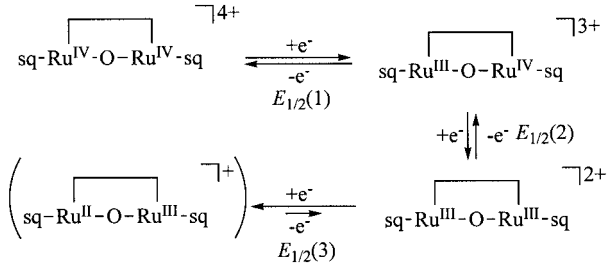

Scheme 4. Redox behavior of $[\mathbf{2}]^{3+}$ in CH_2Cl_2.

The changes of the oxidation states of $[\mathbf{2}]^{3+}$ were followed by UV/Vis/NIR spectroscopy. The one-electron oxidation of $[\mathbf{2}]^{3+}$ at +0.80 V resulted in disappearance of the bands at 1333 and 766 nm and generation of a new band at 656 nm. The electrochemical reduction of $[\mathbf{2}]^{3+}$ at –0.25 V also caused a disappearance of the same bands and the generation of a strong band at 872 nm (Figure 5). These spectral changes between $[\mathbf{2}]^{2+}$, $[\mathbf{2}]^{3+}$, and $[\mathbf{2}]^{4+}$ occur reversibly depending on the electrolysis potentials.

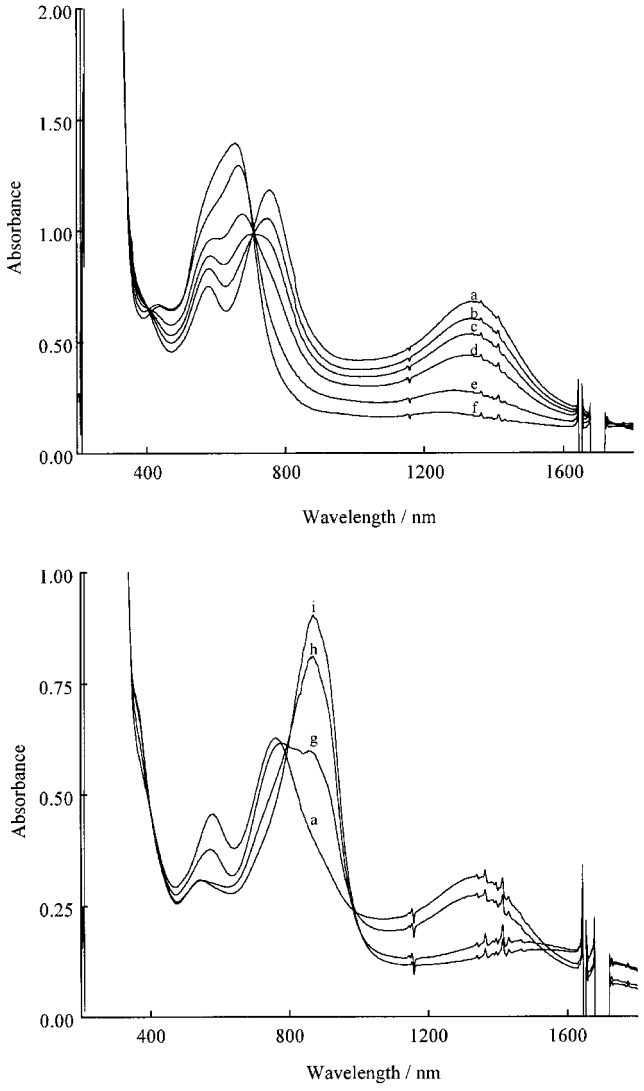

Figure 5. UV/Vis/NIR spectra of [**2**](PF$_6$)$_3$: a) before electrolysis and after electrolysis at b) +0.40 V, c) +0.50 V, d) +0.60 V, e) +0.70 V, f) +0.80 V, g) +0.00 V, h) –0.10 V, and i) –0.25 V in CH_2Cl_2 containing nBu$_4$NClO$_4$ (0.1 M) as an electrolyte.

If [**2**]$^{2+}$ has the [(sq)Ru^{III}–O–Ru^{III}(sq)]$^{2+}$ core, the monocation [**2**]$^{+}$ would also be a mixed-valence metal complex. The controlled potential electrolysis of [**2**]$^{3+}$ at –0.60 V in CH_2Cl_2, however, induced fragmentation reactions of the complex, as re-oxidation of the resultant solution at –0.20 V did not recover the spectrum of [**2**]$^{2+}$.[13] The decomposition of the mixed-valence complex [**2**]$^{+}$ may be caused by the fragility of the Ru^{III}–O–Ru^{II} bond (vide infra). It is worthy of note that the mixed-valence complex [**2**]$^{3+}$, with the [(sq)-Ru^{III}–O–Ru^{IV}(sq)]$^{3+}$ core, is quite stable in solution, since the disproportionation constant of [**2**]$^{3+}$ [Equation (2)] is negligibly small ($K_d = 1.5\times10^{-11}$) in contrast to that of [**1**]$^{+}$ ($K_d = 0.21$).

Redox Behavior of [2]$^{3+}$ in MeOH

The fragility of the highly reduced form of [**2**]$^{3+}$ becomes more prominent in MeOH. In contrast to the CV of [**2**]$^{3+}$ in CH_2Cl_2, the complex exhibits four redox couples in a potential range from +1.0 to –1.0 V in MeOH or CF_3CH_2OH[14] (Figure 6).

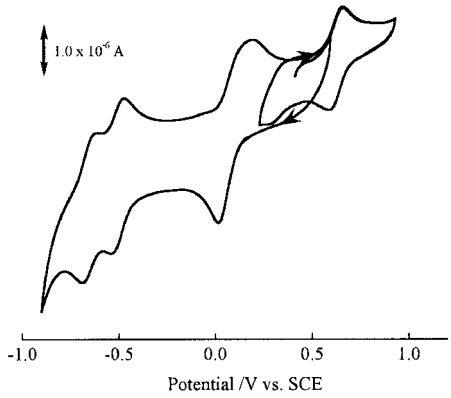

Figure 6. CV of [**2**](PF$_6$)$_3$ in MeOH and CF_3CH_2OH containing nBu$_4$NClO$_4$ (0.1 M) as an electrolyte under N_2. The arrows indicate the rest potentials of the solution and the direction of scan.

The rest potential (E_{rest} = +0.38 V) and the redox potential of the quasi-reversible couple [$E_{1/2}$(1) = +0.66 V] in CF_3CH_2OH are quite close to those in CH_2Cl_2, suggesting the stability of [**2**]$^{4+}$ as well as [**2**]$^{3+}$ in CF_3CH_2OH and MeOH. On the other hand, a peak current of the cathodic wave at E_{pc} = +0.02 V in MeOH is much larger than that of the redox couple at $E_{1/2}$(1) = +0.66 V. Indeed, the controlled potential electrolysis of [**2**]$^{3+}$ at –0.30 V in MeOH consumes 2.96 F mol^{-1} of electricity. Despite the occurrence of such an unusual three-electron reduction of [**2**]$^{3+}$ at E_{pc} = +0.02 V, the pattern of the CV of Figure 6 remained unchanged in multi-potential sweeps in a range of +0.70 V to –0.90 V. We therefore concluded that [**2**]$^{3+}$ undergoes three-electron reduction and oxidation reactions at E_{pc} = +0.02 V and E_{pa} = +0.2 V(broad) in MeOH. The reversible conversion between [**2**]$^{3+}$ and the three-electron oxidation products was also evidenced by the electronic absorption spectra, since the bands of [**2**]$^{3+}$ at 1330 and 766 nm disappeared during the controlled potential electrolysis at –0.30 V in MeOH with generation of two new bands at 848 and 876 nm (Figure 7).

Re-oxidation of the resultant solution at +0.40 V recovered the electronic absorption spectrum of [**2**]$^{3+}$. Taking into account that the three-electron reduction of [**2**]$^{3+}$ takes place at E_{pc} = +0.02 V in MeOH, chemical reduction of [**2**]$^{3+}$ was conducted by treatment with $Na_2S_2O_3$ (excess) in MeOH/H_2O (1:1 v/v) and a dark-purple product was obtained as a PF_6 salt in a 66% yield. The electronic absorption spectra of the product shows two strong CT bands at 848 and 876 nm, suggesting the existence of two types of Ru^{II}(sq) frameworks, and the pattern of the spectrum is fully consistent with that of the electrochemically three-electron-reduced form of [**2**]$^{3+}$ in MeOH. The ESI mass spectra[15] (Figure 8) show a signal at m/z = 738, which corresponds to the summation of the molecular weights of [**2**]^{0} + CH_3OH + H^+ with a composition that is consistent with the elemental analysis of the product.

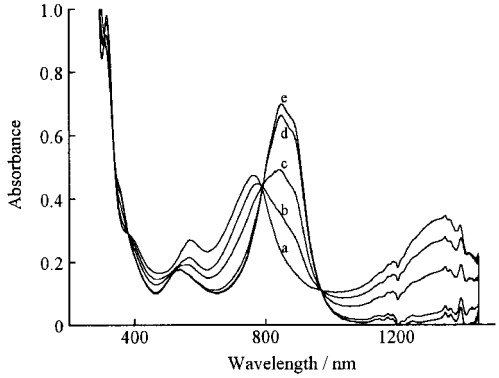

Figure 7. UV/Vis/NIR spectra of [**2**]$(PF_6)_3$: a) before and after electrolysis at b) +0.10 V, c) 0.00 V, d) –0.10 V, and e) –0.20 V in MeOH containing nBu$_4$NClO$_4$ (0.1 M) as an electrolyte under N_2.

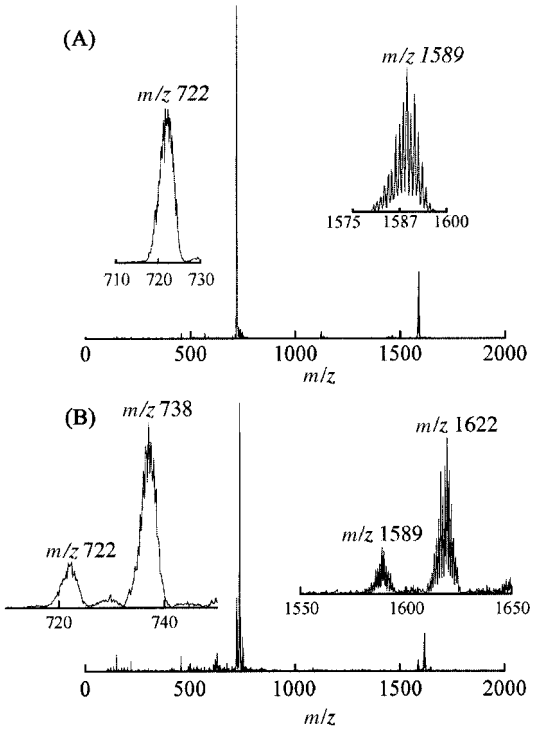

Figure 8. ESI mass spectra of (A) [**2**]$(PF_6)_3$ and (B) [**3**](PF_6) in MeOH.

Based on a combination of the ESI-MS measurements and the UV/Vis/NIR spectra, the most reasonable structure of the product is [{$Ru^{II}(OH_2)$(3,6-tBu$_2$sq)}{Ru^{II}(OMe)(3,6-tBu$_2$sq)}(btpyxa)](PF_6) {[**3**](PF_6)} [Equation (3)].

$$\left[(sq)Ru^{III}\text{–}O\text{—}Ru^{IV}(sq)\right]^{3+} + 3e^- + H^+ + CH_3OH \rightleftharpoons \left[(sq)Ru^{II}(OH_2)\ (MeO)Ru^{II}(sq)\right]^{+} \quad (3)$$

[**2**]$^{3+}$ [**3**]$^{+}$

Chemical reduction of [**2**]$^{3+}$ with a large excess of $Na_2S_2O_3$ in CF_3CH_2OH in place of MeOH gave only [**2**]$^{2+}$ on the basis of ESI-MS and UV/Vis/NIR measurements; the monocationic dimer bearing Ru–OH and Ru–OCH_2CF_3 moieties was not detected at all in the reaction mixtures. The cavity generated by btpyxa may be too small for an attack of CF_3CH_2OH at Ru.

It is worthy of note that the conversion between [**2**]$^{3+}$ and [**3**]$^{+}$ triggered by the three-electron redox reaction takes place reversibly on the CV timescale. Such an unusual reaction can be explained in terms of the fragility of the Ru^{II}–O–Ru^{III} and Ru^{II}–O–Ru^{II} frameworks and the stability of the Ru^{III}–O–Ru^{III} and Ru^{III}–O–Ru^{IV} ones due to the strong electron-donating ability of the μ-oxo ligand. In addition, the flexibility of the btpyxa ligand must play a key role in the smooth μ-oxo bond formation and cleavage reactions. Degradation of the two-electron-reduced form of [**2**]$^{3+}$ ([**2**]$^{+}$) in CH_2Cl_2, therefore, is correlated with the lability of the Ru^{II}–O–Ru^{III} group of [**2**]$^{+}$ in MeOH.

A proposed mechanism for the formation of [**3**]$^{+}$ is depicted in Scheme 5. A one-electron reduction of [**2**]$^{3+}$ at +0.02 V in MeOH will induce protonation of the bridging O atom of [**2**]$^{2+}$, which causes an anodic shift of the reduction potential of the resultant [(sq)Ru^{III}–O(H)–Ru^{III}-(sq)]$^{3+}$. As a result, the latter undergoes further one-electron reduction to generate [(sq)Ru^{II}–O(H)-Ru^{III}(sq)]$^{2+}$ at the same potential. Taking into account that [(sq)Ru^{II}–O–Ru^{III}(sq)]$^{+}$ is not stable in CH_2Cl_2, the Ru–O(H)–Ru bond of [(sq)Ru^{II}–O(H)–Ru^{III}(sq)]$^{2+}$ will be immediately cleaved and the resultant vacant coordination site of Ru attacked by MeOH, which is accompanied by protonation of the Ru–OH group. Such protonation would also cause an anodic shift of the reduction potential of the [{$Ru^{III}(OH_2)$-(sq)}{Ru^{II}(OMe)(sq)}]$^{2+}$ framework. Thus, simultaneous three-electron reduction of [**2**]$^{3+}$ in MeOH is ascribed to a successive one-electron reduction coupled with proton transfer.

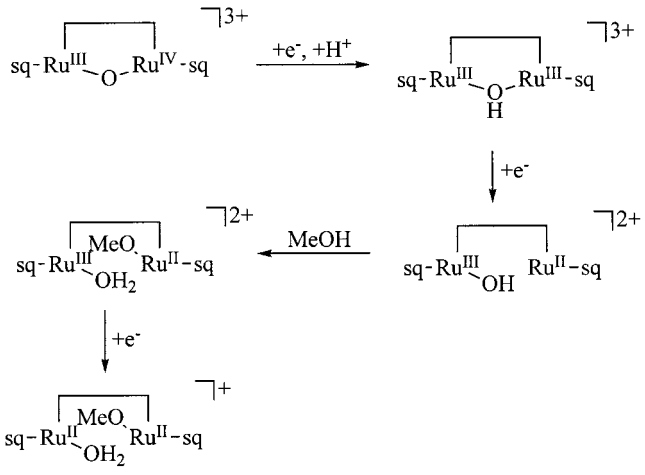

Scheme 5. A proposed mechanism for the reduction of [**2**]$^{3+}$ in MeOH.

The distance between the carbons at the 4- and 5-positions of btpyxa was determined as 4.56 Å by an X-ray structural analysis of [PtCl(btpyxa)]$^{+}$, in which the xanthene skeleton is planar probably due to π-π stacking of two

trpy planes.[9] On the other hand, the Ru···Ru interatomic distance and the Ru–O–Ru bond angle of the oxo-bridged dimer $[(bpy)_2(OH_2)Ru–O–Ru(OH_2)(bpy)_2]^{4+}$ are 3.708(1) Å and 165.4(3)°.[16] The xanthene framework in the present μ-oxo dimers, therefore, must deviate largely from linear in order to accept two Ru(sq)(trpy) moieties connected by the μ-oxo bond. On the contrary, dinuclear Ru complexes bridged by btpyan, with the rigid anthracene plane, are practically impossible to fit bent Ru–O–Ru bonds. This view reasonably explains why ruthenium dimers bridged by btpyxa form μ-oxo bonds whereas those with btpyan cannot accommodate a bent Ru–O–Ru bond. The unusual simultaneous three-electron redox reaction of $[\mathbf{2}]^{3+}$, which is accompanied by the formation and cleavage of the oxo bridge connecting the two [Ru(trpy)(sq)] frameworks, is therefore ascribed to the synergic effects of participation of proton transfer in the redox reaction, the flexibility of btpyxa, and the high affinity of the μ-oxo bond for high oxidation states of Ru.

Conclusions

Bis(chlororuthenium–semiquinone) $[\mathbf{1}](PF_6)_2$ and μ-oxobis(ruthenium–semiquinone) $[\mathbf{2}](PF_6)_3$ complexes, bridged with btpyxa, have been prepared and their redox behavior investigated. The electronic states of $[\mathbf{1}](PF_6)_2$ and $[\mathbf{2}](PF_6)_3$ were expressed by $[(sq)ClRu^{III}–Ru^{III}Cl(sq)]^{2+}$ and $[(sq)Ru^{III}–O–Ru^{IV}(sq)]^{3+}$, respectively, based on the ESI-MS, elemental analysis, and UV/Vis/NIR spectra. Dicationic $[\mathbf{1}]^{2+}$ undergoes two successive metal-centered one-electron reactions and a ligand-based simultaneous two-electron redox reaction at $E_{1/2}$ = +0.13, +0.09, and –0.75 V (vs. SCE), respectively, in CH_2Cl_2. The mixed-valence state of $[\mathbf{2}]^{3+}$ is quite stable because the ruthenium–semiquinone moieties of $[\mathbf{2}]^{3+}$ interact strongly with each other through the oxo bridge. The mixed-valence complex $[\mathbf{2}]^{3+}$ can be reversibly oxidized and reduced to and from the $Ru^{IV}–Ru^{IV}$ and $Ru^{III}–Ru^{III}$ oxidation states at $E_{1/2}$ = +0.63 and –0.01 V, respectively in CH_2Cl_2. On the other hand, $[\mathbf{2}]^{3+}$ undergoes a three-electron reduction accompanied by cleavage of the Ru–O–Ru bond at E_p = +0.02 V, and $[\{Ru(OMe)(3,5\text{-}tBu_2sq)\}\{Ru(OH_2)(3,5\text{-}tBu_2sq)\}(btpyxa)]^+$ is formed in MeOH. The unusual reversible Ru–O–Ru bond cleavage and formation during the three-electron redox reaction can be ascribed not only to the stability and fragility of the μ-oxo bond at high and low oxidation states of the Ru centers, respectively, but also to the flexibility of btpyxa.

Experimental Section

General Remarks: $RuCl_3·3H_2O$ was purchased from Furuya Metal Co., Ltd., NH_4PF_6 and $Na_2S_2O_3$ from Wako Pure Chemical industries, Ltd. 3,6-Di-*tert*-butylcatechol[17] and btpyxa[9] were synthesized according to literature procedures. All solvents were purified by distillation.

UV/Vis/NIR spectra were recorded on a Shimazu UVPC-3100 UV/Vis/NIR scanning spectrophotometer. ESI mass spectra were measured with a Shimazu LCMS-2010 liquid chromatograph mass spectrometer and Waters Micromass LCT. Elemental analyses were carried out at the Research Center for Molecular-Scale Nanoscience. Cyclic voltammetry (CV) was performed with an ALS/Chi model 660 electrochemical analyzer. CVs were recorded in CH_2Cl_2 or MeOH containing 0.1 mol dm^{-3} of nBu$_4$NClO$_4$ as an electrolyte at a scan rate of 50 mV s^{-1} at 298 K using a glassy carbon disk as the working electrode, a Pt wire as the counter electrode, and Ag/$AgNO_3$ (0.01 M) as the reference electrode. All potentials were converted to SCE ($E_{SCE} = E_{Ag/Ag+} + 0.330$ V). Spectroelectrochemical measurements of UV/Vis/NIR spectra were conducted in CH_2Cl_2 or MeOH containing 0.1 mol dm^{-3} of nBu$_4$NClO$_4$ as an electrolyte using a thin-layer optical cell (path length: 0.5 mm) with a platinum minigrid working electrode sandwiched between the two glass sides of an optical cell, a platinum counter electrode, and an Ag/$AgNO_3$ reference electrode. A Hokuto Denko HA-501 potentiostat and a Shimazu UV-3100PC UV/Vis/NIR scanning spectrophotometer were used. Controlled-potential electrolysis was carried out in CH_2Cl_2 or MeOH at room temperature under N_2 in an electrolysis cell consisting of three compartments: one for the glassy carbon plate (15 mm × 30 mm), the second for a platinum counter electrode (15 mm × 30 mm), which was separated from the working electrode cell by an anion-exchange membrane, and the third for an Ag/$AgNO_3$ reference electrode.

$[Ru_2Cl_6(btpyxa)]$: A dehydrated MeOH solution (30 mL) containing $RuCl_3·3H_2O$ (133 mg, 0.50 mmol) and btpyxa (200 mg, 0.25 mmol) was deoxygenated with a stream of nitrogen gas for 30 min and the solution was then refluxed for 3 h under N_2. The dark brown solid precipitate was filtered off and washed with MeOH (5 mL, three times) and acetone (5 mL, three times) to remove unreacted $RuCl_3$ and btpyxa, and then dried in vacuo. Yield: 204 mg (68%). $C_{53}H_{48}Cl_6N_6ORu_2$ (1199.9): calcd. C 53.05, H 4.03, N 7.00; found C 53.12, H 4.11, N 6.82.

$[Ru_2Cl_2(3,6\text{-}tBu_2sq)_2(btpyxa)](PF_6)_2$ $\{[\mathbf{1}](PF_6)_2\}$: An MeOH suspension (30 mL) containing $[Ru_2Cl_6(btpyxa)]$ (200 mg, 0.17 mmol) and 3,6-di-*tert*-butylcatechol (83 mg, 0.37 mmol) was deoxygenated with a stream of nitrogen gas for 30 min in a 100-mL flask. A deoxygenated MeOH solution (30 mL) of *t*BuOK (124 mg, 1.11 mmol) was then added to the suspension by syringe under N_2 and the reaction mixture was stirred for 24 h at room temperature under N_2. Insoluble $[Ru_2Cl_6(btpyxa)]$ gradually dissolved and the solution became dark-purple. The reaction mixture was then exposed to air. The dark-purple solution turned dark-blue in color in 2 h. After evaporation of the solution to dryness under reduced pressure, the product was purified by column chromatography using Alumina N super-I (ICN Biomedicals GmbH) and acetone/EtOH as an eluent. An aqueous solution of NH_4PF_6 was added to the dark-blue fraction. Concentration of the solution under reduced pressure gave a dark-blue powder, which was separated by filtration and dried in vacuo. Yield: 97 mg (32%). ESI-MS: m/z = 749 ($[\mathbf{1}]^{2+}$). $C_{81}H_{88}Cl_2F_{12}N_6O_5P_2Ru_2$ (1788.6): calcd. C 54.39, H 4.96, N 4.70; found C 54.40, H 5.01, N 4.66.

$[Ru_2(\mu\text{-}O)Cl_4(btpyxa)]·3H_2O$: An MeOH/$H_2O$ (80:20) solution (30 mL) containing $RuCl_3·3H_2O$ (133 mg, 0.50 mmol) and btpyxa (200 mg, 0.25 mmol) was deoxygenated with a stream of nitrogen gas for 30 min, after which time the solution was heated at reflux for 3 h under N_2. The dark-brown hot solution was filtered and evaporated to 10 mL under reduced pressure. The brown solid precipitate was filtered off and washed with cold MeOH (1 mL, three times) to remove unreacted $RuCl_3$ and btpyxa. Yield: 195 mg (65%). $C_{53}H_{54}Cl_4N_6O_5Ru_2$ (1199.0): calcd. C 53.09, H 4.54, N 7.01; found C 52.21, H 4.52, N 6.88.

$[Ru_2(\mu\text{-}O)(3,6\text{-}t\text{Bu}_2\text{sq})_2(\text{btpyxa})](PF_6)_3$ {[2]$(PF_6)_3$}: An MeOH solution (30 mL) containing $[Ru_2(\mu\text{-}O)Cl_4(\text{btpyxa})]$ (150 mg, 0.13 mmol) and 3,6-di-*tert*-butylcatechol (63 mg, 0.29 mmol) was deoxygenated with a stream of nitrogen gas for 30 min in a 100-mL flask. A deoxygenated MeOH solution (50 mL) of KOAc (852 mg, 8.7 mmol) was then added to the solution by syringe under N_2. The reaction mixture was stirred for 24 h at room temperature under N_2. The reaction mixture gradually turned dark-purple, and it was then exposed to air. The solution's color turned black in 2 h. After evaporation of the solution to dryness under reduced pressure, an aqueous solution of NH_4PF_6 was added to the methanolic solution (5 mL) of the residue. The resultant black powder was filtered and purified by column chromatography using Alumina N super-I (ICN Biomedicals GmbH) and CH_2Cl_2 as the eluent. Evaporation of acetone from the black fraction gave a black powder, which was filtered and dried in vacuo. Yield: 25 mg (11%). ESI-MS: *m*/*z* = 1589 $\{[\mathbf{2}](PF_6)\}^+$, 722 ($[\mathbf{2}]^{2+}$), 481 ($[\mathbf{2}]^{3+}$).[15] $C_{81}H_{88}F_{18}N_6O_6P_3Ru_2$ (1794.6): calcd. C 51.79, H 4.72, N 4.47; found C 51.64, H 4.80, N 4.65.

Chemical Reduction of [2]$(PF_6)_3$: An aqueous solution (5 mL) of $Na_2S_2O_3$ (10 mg, excess) was added to an MeOH solution (5 mL) of [**2**]$(PF_6)_3$ (10 mg, 5.6 μmol) and the solution was stirred for a few minutes. Evaporation of the solution under reduced pressure precipitated a dark-purple powder of [{Ru(OMe)(3,6-$t\text{Bu}_2$sq)}-{Ru(OH_2)(3,6-$t\text{Bu}_2$sq)}(btapyxa)](PF_6) {[**3**](PF_6)}, which was filtered and dried in vacuo. Yield: 6 mg (66%). ESI-MS: *m*/*z* = 1622 $\{[\mathbf{3}](PF_6)\}^+$, 738 ($[\mathbf{3}]^{2+}$).[13] $C_{82}H_{92}F_6N_6O_7PRu_2$ (1620.8): calcd. C 60.73, H 5.78, N 5.18; found C 60.62, H 5.80, N 4.98.

Acknowledgments

We are grateful to Dr. Hideo Kakimi and Dr. Hiroshi Yamasu of Jasco International Co., Ltd. for the ESI-TOF MS measurements.

[1] a) C. R. Pierpont, *Coord. Chem. Rev.* **2001**, *216–217*, 99–125; b) A. B. P. Lever, S. I. Gorelsky, *Coord. Chem. Rev.* **2000**, *208*, 153–167; c) S. I. Gorelsky, E. S. Dodsworth, A. B. P. Lever, A. A. Vlcek, *Coord. Chem. Rev.* **1998**, *174*, 469–494.

[2] a) C. Carbonera, A. Dei, C. Sangregorio, J.-F. Létard, *Chem. Phys. Lett.* **2004**, *396*, 198–201; b) P. Gütlich, A. Dei, *Angew. Chem. Int. Ed. Engl.* **1997**, *36*, 2734–2736; c) D. A. Shultz, in *Magnetism: Molecules to Materials* (Eds.: J. S. Miller, M. Drillon), Wiley-VCH, Weinheim, **2001**, p. 281.

[3] a) K. Yamada, S. Yagishita, H. Tanaka, K. Tohyama, K. Adachi, S. Kaizaki, H. Kumagai, K. Inoue, R. Kitaura, H.-C. Chang, S. Kitagawa, S. Kawata, *Chem. Eur. J.* **2004**, *10*, 2647–2660; b) M. Oh, G. B. Carpenter, D. A. Sweigart, *Acc. Chem. Res.* **2004**, *37*, 1–11; c) W. Paw, J. B. Keister, C. H. Lake, M. R. Churchill, *Organometallics* **1995**, *14*, 767–779.

[4] a) M. Ebadi, A. B. P. Lever, *Inorg. Chem.* **1999**, *38*, 467–474; b) K. Yang, J. A. Martin, S. G. Bott, M. G. Richmond, *Inorg. Chim. Acta* **1997**, *254*, 19–27; c) R. S. da Silva, E. Tfouni, A. B. P. Lever, *Inorg. Chim. Acta* **1995**, *235*, 427–430; d) A. B. P. Lever, H. Masui, R. A. Metcalfe, D. J. Stufkens, E. S. Dodsworth, P. R. Auburn, *Coord. Chem. Rev.* **1993**, *125*, 317–331; e) N. Bag, G. K. Lahiri, P. Basu, A. Chakravorty, *J. Chem. Soc., Dalton Trans.* **1992**, 113–117; f) N. Bag, A. Pramanik, G. K. Lahiri, A. Chakravorty, *Inorg. Chem.* **1992**, *31*, 40–45; g) S. Bhattacharya, C. G. Pierpont, *Inorg. Chem.* **1991**, *30*, 1511–1516; h) H. Masui, A. B. P. Lever, P. R. Auburn, *Inorg. Chem.* **1991**, *30*, 2402–2410; i) P. R. Auburn, E. S. Dodsworth, M. Haga, W. Liu, W. A. Nevin, *Inorg. Chem.* **1991**, *30*, 3502–3512; j) S. R. Boone, C. G. Pierpont, *Polyhedron* **1990**, *9*, 2267–2272; k) M. Haga, K. Isobe, S. R. Boone, C. G. Pierpont, *Inorg. Chem.* **1990**, *29*, 3795–3799; l) D. J. Stufkens, Th. L. Snoeck, A. B. P. Lever, *Inorg. Chem.* **1988**, *27*, 953–956; m) A. B. P. Lever, P. R. Auburn, E. S. Dodsworth, M. Haga, W. Liu, M. Melnik, W. A. Nevin, *J. Am. Chem. Soc.* **1988**, *110*, 8076–8084; n) S. R. Boone, C. G. Pierpont, *Inorg. Chem.* **1987**, *26*, 1769–11773; o) M. Haga, E. S. Dodsworth, A. B. P. Lever, *Inorg. Chem.* **1986**, *25*, 447–453; p) M. Haga, E. S. Dodsworth, A. B. P. Lever, S. R. Boone, C. G. Pierpont, *J. Am. Chem. Soc.* **1986**, *108*, 7413–7414; q) R. B. Salmonsen, A. Abelleira, M. J. Clarke, S. D. Pell, *Inorg. Chem.* **1984**, *23*, 385–387.

[5] a) M. Kurihara, S. Daniele, K. Tsuge, H. Sugimoto, K. Tanaka, *Bull. Chem. Soc. Jpn.* **1998**, *71*, 867–875; b) K. Tsuge, K. Tanaka, *Chem. Lett.* **1998**, 1069–1070; c) K. Tsuge, M. Kurihara, K. Tanaka, *Bull. Chem. Soc. Jpn.* **2000**, *73*, 607–614.

[6] a) K. Kobayashi, H. Ohtsu, T. Wada, K. Tanaka, *Chem. Lett.* **2002**, 868–869; b) K. Kobayashi, H. Ohtsu, T. Wada, T. Kato, K. Tanaka, *J. Am. Chem. Soc.* **2003**, *125*, 6729–6739.

[7] a) H. Sugimoto, K. Tanaka, *J. Organomet. Chem.* **2001**, *622*, 280–285; b) T. Wada, T. Fujihara, M. Tomori, D. Ooyama, K. Tanaka, *Bull. Chem. Soc. Jpn.* **2004**, *77*, 741–749.

[8] a) T. Wada, K. Tsuge, K. Tanaka, *Angew. Chem.* **2000**, *112*, 1542–1545; *Angew. Chem. Int. Ed.* **2000**, *39*, 1479–1482; b) T. Wada, K. Tsuge, K. Tanaka, *Inorg. Chem.* **2001**, *40*, 329–337.

[9] R. Okamura, T. Wada, K. Aikawa, T. Nagata, K. Tanaka, *Inorg. Chem.* **2004**, *43*, 7210–7217.

[10] The difference in the redox potential between the $[\mathbf{1}]^{2+}$/ $[\mathbf{1}]^+$ and $[\mathbf{1}]^+$ /$[\mathbf{1}]^0$ couples ($\Delta E_{1/2}$ = 0.04 V) is too small to form pure $[\mathbf{1}]^+$ in the bulk electrolysis. So, bulk electrolysis was conducted at 0 V. Accordingly, disproportionation of $[\mathbf{1}]^+$ to $[\mathbf{1}]^{2+}$ and $[\mathbf{1}]^0$ [Equation (1)] has no influence on the number of electrons consumed in the electrolysis.

[11] C. L. Bird, A. T. Kuhn, *Chem. Soc. Rev.* **1981**, *10*, 49–82.

[12] R. W. Callahan, G. M. Brown, T. J. Meyer, *Inorg. Chem.* **1975**, *14*, 1443–1453.

[13] The controlled-potential electrolysis of $[\mathbf{2}]^{2+}$ at –0.60 V in CH_2Cl_2 resulted in disappearance of the 872-nm band of $[\mathbf{2}]^{2+}$ and generation of a weak, broad band at 864 nm. Re-oxidation of the solution at –0.25 V, however, did not recover the spectrum of $[\mathbf{2}]^{2+}$ nor produce any strong absorption bands in the visible region. This result implies the dissociation of the dioxolene ligands of $[\mathbf{2}]^+$ during the electrochemical reduction.

[14] CF_3CH_2OH was used as a solvent for the CV of $[\mathbf{2}]^{3+}$ instead of MeOH because MeOH is oxidized above ca. +0.8 V in the conditions of CV.

[15] The trication was not detected in the ESI mass spectrum of [**2**]$(PF_6)_3$ in MeOH or CH_2Cl_2 using a normal electrospray ionization probe because $[\mathbf{2}]^{3+}$ is readily reduced to $[\mathbf{2}]^{2+}$ under the experimental conditions used. The signals of $[\mathbf{2}]^{3+}$ were, however, detected as a cluster ion with solvent at 30 °C by ESI-TOF MS employing a Nanoflow-ESI probe with an orthogonal acceleration time-of-flight (Waters–Micromass). The monocation was not detected in the ESI-mass spectrum of [**3**](PF_6) in MeOH because $[\mathbf{3}]^+$ is readily oxidized to $[\mathbf{3}]^{2+}$, which was detected as the monocation $\{[\mathbf{3}](PF_6)\}^+$.

[16] J. A. Gilbert, D. S. Eggleston, W. R. Murphy Jr., D. A. Geselowitz, S. W. Gersten, D. J. Hodgson, T. J. Meyer, *J. Am. Chem. Soc.* **1985**, *107*, 3855–3864.

[17] I. S. Belostotskaya, N. L. Komissarova, E. V. Dzhuaryan, V. V. Ershov, *Seriya Khimicheskaya* **1972**, *7*, 1594–1596.

Received: February 17, 2005
Published Online: August 17, 2005

